PHYSICAL REVIEW B **81**, 140408(R) (2010)

Nonlinear frequency and amplitude modulation of a nanocontact-based spin-torque oscillator

P. K. Muduli,* Ye. Pogoryelov, and S. Bonetti
Materials Physics, Royal Institute of Technology, Electrum 229, 164 40 Kista, Sweden

G. Consolo
Department of Physics, University of Ferrara, 44100 Ferrara, Italy

Fred Mancoff
Everspin Technologies, Inc., 1300 N. Alma School Road, Chandler, Arizona 85224, USA

Johan Åkerman
Materials Physics, Royal Institute of Technology, Electrum 229, 164 40 Kista, Sweden
and Physics Department, University of Gothenburg, 412 96 Gothenburg, Sweden

(Received 15 October 2009; revised manuscript received 4 March 2010; published 28 April 2010)

We study the current-controlled modulation of a nanocontact spin-torque oscillator. Three principally different cases of frequency nonlinearity (d^2f/dI_{dc}^2 being zero, positive, and negative) are investigated. Standard nonlinear frequency-modulation theory is able to accurately describe the frequency shifts during modulation. However, the power of the modulated sidebands only agrees with calculations based on a recent theory of combined nonlinear frequency and amplitude modulation.

DOI: 10.1103/PhysRevB.81.140408 PACS number(s): 75.75.−c, 85.70.Kh, 85.75.−d, 84.30.Ng

Spin-torque oscillators (STO) offer a combination of attractive properties such as ultrawide band frequency operation,[1,2] extremely small footprint (without any need for large inductors), and easy integration using well-established magnetoresistive random access memory processes. The basic principle of a spin-torque oscillator is based on the transfer of angular momentum from a spin-polarized current to the local magnetization.[3,4] The effect usually occurs in a nanoscale device where a large current density ($\sim 10^8$ A/cm^2) can drive the precession of the free layer magnetization at GHz frequencies,[5,6] thus acting as a nanoscale oscillator. Effective modulation of the microwave signal generated from STOs is required for communication applications. However, both the STO frequency and amplitude are typically nonlinear functions of the drive current. This nonlinearity is related to a change in the precession angle with the increase in the current magnitude.[7–9] Experiments have shown other sources of nonlinearities such as temperature[10] and dynamic-mode hopping.[11–13] The wide range of possible sources of nonlinear behavior is likely to render the frequency modulation of STOs highly nontrivial.

Despite the rapidly growing literature on the many different aspects of STOs, experimental studies of frequency modulation are still limited to a single work by Pufall *et al.*[14] They observed both unequal sideband amplitudes and a shift of the carrier frequency with modulation amplitude, which they ascribed to nonlinear frequency modulation (NFM). While linear frequency-modulation (LFM) theory assumes that the instantaneous frequency of the modulated signal is linearly proportional to the modulating signal,[15] NFM theory takes into account the nonlinear change in the intrinsic operating frequency during modulation. Pufall *et al.*[14] calculated the observed sideband amplitudes using NFM theory and found a rather large (about 50%) discrepancy between their calculated and experimentally observed sidebands, which they argued might be due to amplitude modulation or other nonlinear properties of the STO.

In this work we study the frequency and amplitude modulation of a nanocontact STO for various amounts of frequency nonlinearity. The frequency nonlinearity is described by the second derivative of the frequency, f, with respect to the dc bias current, I_{dc}, d^2f/dI_{dc}^2. Three different cases of frequency nonlinearity (d^2f/dI_{dc}^2 being zero, positive, and negative) are investigated. As expected from NFM theory, the carrier and its associated sidebands exhibit a change in frequency under modulation, which can be directly calculated from the experimentally determined nonlinear properties of the frequency of the free-running STO. However, the *power* of the modulated sidebands is only poorly reproduced using NFM theory and we show that it is essential to consider *amplitude* modulation in order to reach any quantitative agreement. Using a recently proposed theory of combined nonlinear frequency and amplitude modulation (NFAM),[16] we are able to show remarkable agreement between our experimental data and calculations, which involve no adjustable parameters. Despite the complex phenomena involved in the STO nonlinearities, we show that modulation of these devices is highly predictable.

The nanocontact metallic-based STOs studied in this work have been described in detail in Ref. 17. Using e-beam lithography, a circular Al nanocontact with nominal diameter of 130 nm is fabricated through a SiO_2 insulating layer, onto a 8×26 μm^2 pseudo-spin-valve mesa with the following layer structure: $Si/SiO_2/Cu(25\ nm)/Co_{81}Fe_{19}(20\ nm)/Cu(6\ nm)/Ni_{80}Fe_{20}(4.5\ nm)/Cu(3\ nm)/Pd(2\ nm)$. While all data presented here has been taken on a single device, similar behavior has been observed in several other devices of the same size.

The low-frequency (100 MHz) modulating current is injected from an RF source to the STO via a circulator. The dc bias current is fed to the device by a precision current source (Keithley 6221) through a dc-40 GHz bias tee connected in parallel with the transmission line. The signal is then amplified using a broadband 16–40 GHz, +22 dB microwave am-

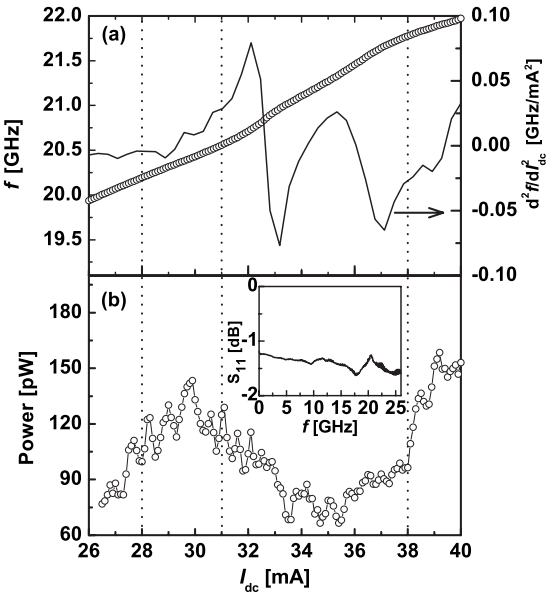

FIG. 1. Current dependence of the free running STO: (a) frequency, f, and its second derivative, d^2f/dI_{dc}^2 and (b) integrated power, both measured in a magnetic field of $H=10$ kOe, applied at 70° to the film plane. Dotted lines indicate the three different operating points (28, 31, and 38 mA) used to compare three principally different cases of frequency nonlinearity, corresponding to d^2f/dI_{dc}^2 being zero, positive, and negative, respectively. Inset in (b) shows the measured S parameter, S_{11} at the STO.

plifier, and finally detected by a spectrum analyzer with an upper frequency limit of 46 GHz (Rohde & Schwarz FSU46). The actual RF current at the STO is calculated by taking into account losses and reflections due to impedance mismatch in the transmission line. Losses in our transmission line and circulator are characterized by injecting an input signal with the microwave source and measuring the output with the spectrum analyzer. The reflection at the STO is measured with a vector network analyzer and is shown in the inset of Fig. 1(b). The scattering matrix element S_{11} shown in the figure is proportional to the amount of reflection at the STO, which is as high as 70–80 % over the entire measured frequency range, 0.01–26 GHz. All other components in the transmission line, which have nominal 50 Ω impedance, give a relative negligible contribution to the total amount of reflected signal. The signal detected at the spectrum analyzer is finally corrected for standing waves in the transmission line. All data shown in this work have been corrected in order to compensate for all these effects.

The measurements are performed in a magnetic field of 10 kOe applied at an angle of 70° to the film plane to ensure that (i) the STO operates around its maximum output power[2] and (ii) only the so-called propagating mode[18–20] is excited. This mode has a higher frequency than the ferromagnetic resonance mode and shows a blueshift with bias current as confirmed in Fig. 1(a). Figure 1 also shows that both the operating frequency and the integrated output power (which is proportional to the actual precession amplitude of the STO) [Fig. 1(b)] are strongly nonlinear functions of the dc bias current. This behavior is likely related to the excitation of closely spaced discrete dynamic modes as the bias current is increased.[11–13]

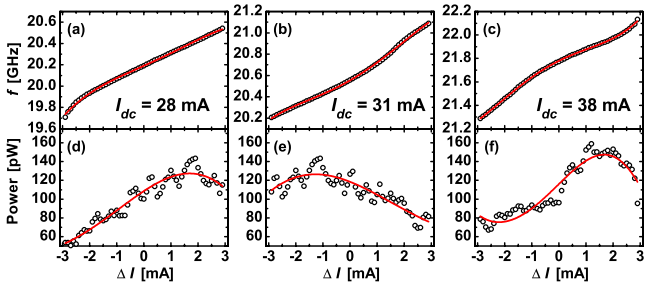

FIG. 2. (Color online) Frequency and integrated power of the free-running STO around the dc bias current values of [(a) and (d)] 28 mA, [(b) and (e)] 31 mA, and [(c) and (f)] 38 mA. The corresponding fourth-order polynomial fits to frequency and the third-order polynomial fits to power are shown in solid red lines.

To test different nonlinear modulation theories, we have chosen to focus on three principally different nonlinear situations described by three different values of d^2f/dI_{dc}^2: zero, positive, and negative, corresponding to a drive current of 28, 31, and 38 mA, respectively. These three operating points are shown as dotted lines in Fig. 1. The nonlinearity can be more clearly seen in Fig. 2, which shows the frequency and integrated power of the free-running STO around these dc bias current values in a range equal to the maximum modulation current. The shape of frequency vs current at 28 mA is almost linear while it is convex for 31 mA and concave for 38 mA. The amplitude sensitivity is also clearly different at these current values, as seen from the corresponding plots of integrated power in Figs. 2(d)–2(f). Around these operating points we modulate the STO using a 100 MHz RF signal swept from 0 to 3 mA. The corresponding spectra are shown in Fig. 3 as a function of the modulating current amplitude. In all three cases, the number of sidebands increases with increasing modulation amplitude. In the case of a linear frequency dependence (28 mA, $d^2f/dI_{dc}^2=0$) the carrier and sideband frequencies are entirely independent of the modulating current (up to a modulation current of 2 mA). In contrast, both the carrier and the sideband frequencies show a clear blueshift at 31 mA and a clear redshift at 38 mA as expected from the finite d^2f/dI_{dc}^2 with opposite signs.

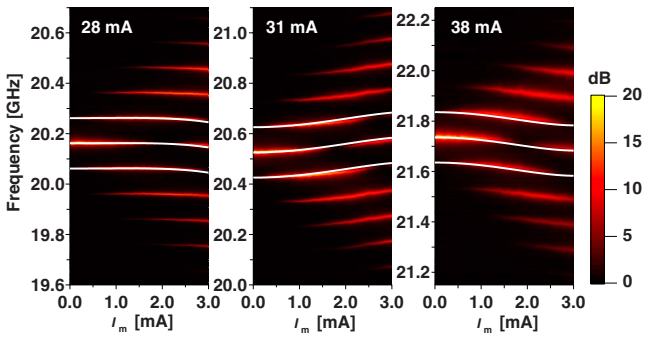

FIG. 3. (Color online) Frequency modulation ($f_m=100$ MHz) of the STO showing the progressive development of sidebands with increasing modulating amplitude I_m at dc bias current values of 28, 31, and 38 mA. Power is expressed in dB over the noise floor. The white lines show the calculated frequency of the carrier and the first-order sidebands according to the combined NFAM theory.

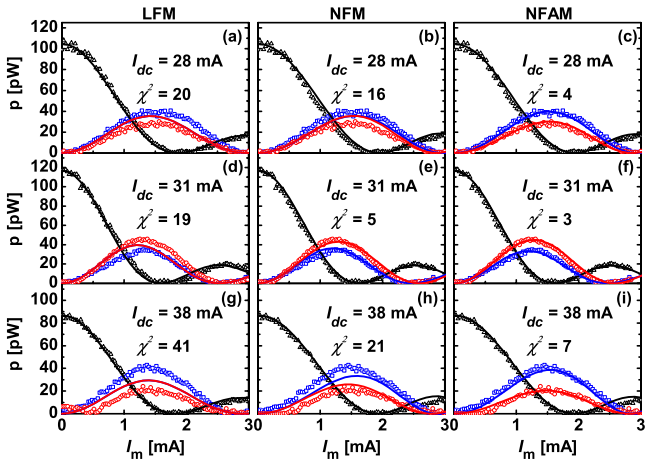

FIG. 4. (Color online) Integrated power of the carrier (black triangles), and the first-order upper (blue squares) and lower (red circles) sidebands for the three different dc bias currents: rows (a)–(c) 28 mA, rows (d)–(f) 31 mA, and rows (g)–(h) 38 mA. First, second, and third columns show the corresponding calculated integrated power (solid lines) as predicted by LFM, NFM, and NFAM, respectively. The mean-square error, χ^2 between the experiment and calculated results of the two sidebands improved significantly for NFAM.

In Fig. 4, we show the detailed modulation current dependence of the carrier and the first-order sideband power with calculated results as described in the following paragraph. While the evolution of the carrier power with modulation current does not seem to be affected by the nonlinearity, both the upper and lower sidebands are strongly affected by the sign and the value of $d^2f/dI_{\rm dc}^2$: the lower sideband gets markedly *stronger* than the upper sideband for $d^2f/dI_{\rm dc}^2>0$ (31 mA), and *weaker* than the upper sideband for $d^2f/dI_{\rm dc}^2<0$ (38 mA). The position of the maximum sideband power is also shifted up/down for the upper/lower sideband. It is noteworthy that this shift only depends on the magnitude of $d^2f/dI_{\rm dc}^2$ and does not change sign when $d^2f/dI_{\rm dc}^2$ goes from positive to negative. Even for the linear case (28 mA, $d^2f/dI_{\rm dc}^2=0$), the power of the two sidebands are unequal. The upper sideband has higher power than the lower sideband, as expected from the positive slope of amplitude versus bias current in Fig. 2(d). This case of linear frequency modulation provides a strong experimental evidence that amplitude modulation is also taking place.

In order to interpret the observed behavior and estimate the importance of both the frequency and amplitude nonlinearities, we consider three qualitatively different models describing (i) LFM, (ii) NFM, and (iii) NFAM. The latter model is adapted from[16] and specifically takes into account nonlinearities in both output frequency and amplitude as a function of the input bias current.

Since LFM and NFM models have already been described in Ref. 14 and 15, we focus on the details of the NFAM model used in our analysis. The instantaneous frequency is assumed to depend nonlinearly on the modulating signal

$$f_i(t) = k_0 + k_1 m(t) + k_2 m(t)^2 + k_3 m(t)^3 + \cdots, \qquad (1)$$

where, $m(t)$, is the modulating signal and the coefficients k_i represent the ith order frequency sensitivity coefficients. Similarly, the output amplitude, A_c is given by

$$A_c(t) = \lambda_0 + \lambda_1 m(t) + \lambda_2 m(t)^2 + \lambda_3 m(t)^3 + \cdots, \qquad (2)$$

where λ_i is ith order amplitude sensitivity coefficient. The coefficients k_i and λ_i are given by the nonlinear current dependence of f and A of the free running STO. We use sine wave modulation, $m(t)=I_m \sin(2\pi f_m t)$, where I_m is the amplitude and f_m is the frequency of modulating signal. The resulting NFAM spectrum becomes[16]

$$\begin{aligned} S(f) = \frac{1}{4}\sum_{h=0}^{3} \gamma_h \sum_{n,m,p,q=-\infty}^{\infty} & J_n(\beta_1)J_m(\beta_2)J_p(\beta_3)J_q(\beta_4) \\ & \times\{\delta[f - f_c^I - (n+2m+3p+4q+h)f_m] \\ & + \delta[f - f_c^I - (n+2m+3p+4q-h)f_m] \\ & + \delta[f + f_c^I - (n+2m+3p+4q+h)f_m] \\ & + \delta[f + f_c^I - (n+2m+3p+4q-h)f_m]\}, \end{aligned} \qquad (3)$$

where $\beta_1=k_1I_m/f_m+3k_3I_m^3/4f_m$, $\beta_2=k_2I_m^2/4f_m+k_4I_m^4/4f_m$, $\beta_3=k_3I_m^3/12f_m$, and $\beta_4=k_4I_m^4/32f_m$ are frequency-modulation indices of different order. $\gamma_0=\lambda_0+\lambda_2I_m^2/2$, $\gamma_1=\lambda_1I_m+3\lambda_3I_m^3/4$, $\gamma_2=\lambda_2I_m^2/2$, and $\gamma_3=\lambda_3I_m^3/4$ are amplitude-modulation parameters. In the above we assumed that the frequency in Eq. (1) is nonlinear up to fourth order and the amplitude in Eq. (2) is nonlinear up to third order, which is found sufficient to describe the experimental data. The frequency spectrum $S(f)$ consists of a *shifted* carrier frequency

$$f_c^I = k_0 + k_2 I_m^2 + 3k_4 I_m^4/8 + \cdots \qquad (4)$$

and an infinite number of sidebands symmetrically located at $f_c^I \pm lf_m$, where $l=n+2m+3p+4q\pm h$ is a positive integer identifying the sideband order. The NFAM carrier shift is identical to that obtained from an NFM model since effects due to amplitude modulation do not enter in Eq. (4). This shift can be readily calculated by means of the polynomial fitting procedure shown in Fig. 2. The comparison with the experimentally obtained values reveals a good agreement, as shown in Fig. 3. The sideband power, on the other hand, is strongly affected by the amplitude modulation, through the coefficients γ_i, and can be used to compare the NFM and NFAM models. In a 6 mA interval around each operating point, we expand the frequency dependence into a fourth-order Taylor series, and the amplitude dependence into a third-order Taylor series as shown in Fig. 2. The coefficients along with their standard errors are summarized in Table I. Using these coefficients we calculate the sideband power expected from NFM and NFAM, respectively, (second and third columns in Fig. 4) and also compare with LFM theory (first column in Fig. 4).

LFM theory completely fails to describe the strong asymmetry between the upper and lower sidebands in all cases. In the linear case of 28 mA [Figs. 4(a)–4(c)] both NFM and LFM theory predict nearly the same behavior with equal sideband power since only k_1 is significant and $k_2\approx 0$. In contrast, the NFAM model correctly produces both the upper and lower sideband power, implying a much better agreement, mostly captured by the amplitude modulation sensitivity coefficient λ_1. In fact, the mean-square error, χ^2 between

TABLE I. Modulation sensitivity coefficients found from polynomial fits of frequency and amplitude of the free-running STO.

Current (mA)	k_0 (GHz)	k_1 (MHz/mA)	k_2 (MHz/mA^2)	k_3 (MHz/mA^3)	k_4 (MHz/mA^4)	λ_0 (pW$^{1/2}$)	λ_1 (pW$^{1/2}$/mA)	λ_2 (pW$^{1/2}$/mA^2)	λ_3 (pW$^{1/2}$/mA^3)
28	20.185	117 ± 1	1 ± 1	2 ± 0.2	8 ± 1	10.4 ± 0.5	0.9 ± 0.07	-0.2 ± 0.02	-0.03 ± 0.01
31	20.545	147 ± 1	20 ± 1	0.8 ± 0.1	-1 ± 0.1	10.9 ± 0.6	-0.5 ± 0.07	-0.15 ± 0.02	0.02 ± 0.01
38	21.779	115 ± 1	-22.5 ± 0.6	-3.3 ± 0.1	1.6 ± 0.1	10.8 ± 1	1.3 ± 0.07	-0.1 ± 0.02	-0.12 ± 0.01

the experiment and calculated results of the two sidebands decreases by about 80% for NFAM theory compared to LFM. In the two nonlinear cases, the NFM model captures the change in sign of the sideband asymmetry, given by the sign change in k_2, but only yields a partial improvement compared to LFM. On the contrary, when the amplitude sensitivity coefficients are also taken into account the agreement of the calculations with experiment is essentially perfect. This agreement is only obtained when *both* frequency and amplitude nonlinearities are accounted for; both k_2 and λ_1 are significant. For 31 mA (38 mA), the mean-square error between the experiment and calculated results of the two sidebands decreases by about 85% (83%) for NFAM theory compared to LFM and about 10% (36%) compared to NFM theory. We emphasize that none of the presented calculations involve *any* free parameters and are completely determined by the experimentally measured nonlinear current dependences of the free-running STO. The agreement with NFAM was also found to be valid for a range of lower modulation frequencies (down to 40 MHz) over the entire range of dc bias currents. Thus our results show that, as long as both nonlinearities are accounted for, the proposed scheme of combined modulation is able to accurately predict the resulting sideband powers and frequency shifts over a wide range of varying operating conditions. Consequently, the STO behaves as an ordinary RF oscillator and should lend itself to communication applications.

In conclusion, we have carried out a detailed modulation study on a nanocontact STO. In particular, we have studied the impact of different levels of frequency nonlinearity. In the nonlinear cases, both carrier and sidebands frequencies are shifted as a function of the modulation current. Both frequency and amplitude nonlinearities produce a significant asymmetry in the power of the upper and lower sidebands. We find that a combined nonlinear frequency and amplitude-modulation model can accurately describe all our experimental data without any adjustable parameters. The modulation of an STO is therefore predictable and independent of the complex mechanism behind the nonlinearity. The results are significant for the continued development of communication and signal processing applications of spin torque oscillators.

Support from the Swedish Foundation for Strategic Research (SSF), the Swedish Research Council (VR), the Göran Gustafsson Foundation and the Knut and Alice Wallenberg Foundation are gratefully acknowledged. Johan Åkerman is a Royal Swedish Academy of Sciences Research Fellow supported by a grant from the Knut and Alice Wallenberg Foundation. Giancarlo Consolo gratefully thanks support from CNISM through "Progetto Innesco." We thank Randy K. Dumas for critical reading of the manuscript.

*muduli@kth.se

[1] W. H. Rippard, M. R. Pufall, S. Kaka, T. J. Silva, and S. E. Russek, Phys. Rev. B **70**, 100406(R) (2004).
[2] S. Bonetti, P. Muduli, F. Mancoff, and J. Åkerman, Appl. Phys. Lett. **94**, 102507 (2009).
[3] J. C. Slonczewski, J. Magn. Magn. Mater. **159**, L1 (1996).
[4] L. Berger, Phys. Rev. B **54**, 9353 (1996).
[5] M. Tsoi, A. G. M. Jansen, J. Bass, W.-C. Chiang, V. Tsoi, and P. Wyder, Nature (London) **406**, 46 (2000).
[6] S. I. Kiselev, J. C. Sankey, I. N. Krivorotov, N. C. Emley, R. J. Schoelkopf, R. A. Buhrman, and D. C. Ralph, Nature (London) **425**, 380 (2003).
[7] D. Houssameddine *et al.*, Nature Mater. **6**, 447 (2007).
[8] A. N. Slavin and P. Kabos, IEEE Trans. Magn. **41**, 1264 (2005).
[9] A. Slavin and V. Tiberkevich, IEEE Trans. Magn. **45**, 1875 (2009).
[10] S. Petit, C. Baraduc, C. Thirion, U. Ebels, Y. Liu, M. Li, P. Wang, and B. Dieny, Phys. Rev. Lett. **98**, 077203 (2007).
[11] J. C. Sankey, I. N. Krivorotov, S. I. Kiselev, P. M. Braganca, N. C. Emley, R. A. Buhrman, and D. C. Ralph, Phys. Rev. B **72**, 224427 (2005).
[12] I. N. Krivorotov, D. V. Berkov, N. L. Gorn, N. C. Emley, J. C. Sankey, D. C. Ralph, and R. A. Buhrman, Phys. Rev. B **76**, 024418 (2007).
[13] I. N. Krivorotov, N. C. Emley, R. A. Buhrman, and D. C. Ralph, Phys. Rev. B **77**, 054440 (2008).
[14] M. R. Pufall, W. H. Rippard, S. Kaka, T. J. Silva, and S. E. Russek, Appl. Phys. Lett. **86**, 082506 (2005).
[15] S. Haykin, *Communication Systems*, 4th ed. (Wiley, New York, 2001).
[16] G. Consolo, V. Puliafito, G. Finocchio, L. Lopez-Diaz, R. Zivieri, L. Giovannini, F. Nizzoli, G. Valenti, and B. Azzerboni, arXiv:0902.4901, IEEE Trans. Magn. (to be published).
[17] F. B. Mancoff, N. D. Rizzo, B. N. Engel, and S. Tehrani, Appl. Phys. Lett. **88**, 112507 (2006).
[18] J. C. Slonczewski, J. Magn. Magn. Mater. **195**, 261 (1999).
[19] A. Slavin and V. Tiberkevich, Phys. Rev. Lett. **95**, 237201 (2005).
[20] S. Bonetti, V. Tiberkevich, P. Muduli, F. Mancoff, A. Slavin, and J. Åkerman, arXiv:0909.3331 (unpublished).